Peer-reviewed version available at Remote Sens. 2018, 10, 402; doi:10.3390/rs10030402

Article

Hydrological Variability and Changes in the Arctic Circumpolar Tundra and Its Largest Pan-Arctic river Basins from 2002 to 2016

Kazuyoshi Suzuki[1,*], Koji Matsuo[2], Dai Yamazaki[3,1], Kazuhito Ichii[4], Yoshihiro Iijima[5], Fabrice Papa[6] and Tetsuya Hiyama[7]

[1] Japan Agency for Marine-Earth Science and Technology (JAMSTEC), 3173-25 Showamachi, Kanazawa-ku, Yokohama, Kanagawa 236-0001, Japan; skazu@jamstec.go.jp (K.S.); d-yamazaki@jamstec.go.jp (D.Y.)
[2] Geospatial Information Authority of Japan, Kitasato 1-ban, Tsukuba, Ibaraki, 305-0816 Japan; matsuo-k96s4@mlit.go.jp
[3] Institute of Industrial Science, The University of Tokyo, 4-6-1 Komaba, Meguro-ku, Tokyo 153-8505 Japan; yamadai@iis.u-tokyo.ac.jp
[4] Center for Environmental Remote Sensing (CEReS), Chiba University, 1-33, Yayoi-cho, Inage-ku, Chiba 263-8522, Japan; ichii@chiba-u.jp
[5] Graduate School of Bioresources, Mie University, 1577 Kurima-Machiya-Cho, Tsu, Mie, 514-8507, Japan; yiijima@bio.mie-ua.c.jp
[6] Laboratoire d'Etudes en Géophysique et Océanographie Spatiales (LEGOS), Université de Toulouse, IRD, CNES, CNRS, UPS, 31400 Toulouse, France; fabrice.papa@ird.fr
[7] Institute for Space-Earth Environmental Research, Nagoya University, Furo-cho, Chikusa-ku, Nagoya, Aichi 464-8601, Japan; hiyama@nagoya-u.jp
* Correspondence: skazu@jamstec.go.jp; Tel.: +81-45-778-5543

Abstract: The Arctic freshwater budget is critical for understanding the climate in the northern regions. However, the hydrology of the Arctic circumpolar tundra region (ACTR) and the largest pan-Arctic rivers are still not well understood. In the present paper, we analyze the spatiotemporal variations in terrestrial water storage (TWS) of the ACTR, including three of its largest pan-Arctic river basins (Lena, Mackenzie, Yukon), using monthly Gravity Recovery and Climate Experiment (GRACE) data from 2002 to 2016. Together with global land reanalysis, river runoff, and inundation extent area (IEA) data, we identify declining TWS trends throughout the ACTR that we attribute largely to increasing evapotranspiration driven by increasing summer air temperatures. In terms of regional changes, large and significant negative trends in TWS are observed mainly over the North American continent. At basin scale, we show that, in the Lena River basin, the autumnal TWS signal persists until the winter of the following year, while in the Mackenzie River basin, the TWS levels in the autumn and winter has no significant impact on the following year. As global warming is expected to be particularly significant in the northern regions, our results are important for understanding future TWS trends, with possible further decline.

Keywords: arctic hydrological cycle; terrestrial water storage; satellite gravimetry observation; permafrost distribution; global land data assimilation system

1. Introduction

The greatest contribution of freshwater into the Arctic Ocean (approximately 40%) comes from terrestrial rivers, including large ones such as the Lena, Ob, Yenissey, Yukon and Mckenzie Rivers [1]. This inflow greatly influences ocean circulation, winter sea ice cover, and boreal climates. Global warming is expected to be particularly significant in the arctic regions. One indicator of this is the 7% increase in average annual discharge of freshwater from the Yenisei, Lena, Ob, Pechora, Kolyma, and Dvina Rivers, six of the largest in Eurasia, to the Arctic Ocean over the last century [2]. For

example, Shiklomanov and Lammer [3] reported that in 2007, the annual river runoff reached a record high for the period 1936–2007, resulting from a general and continuously increasing trend. Despite several studies, the reason for those observations is not fully understood; this is in part because of the poor surface observation network in the area. Rawlins et al. [4] demonstrated that winter precipitation was highly correlated with the annual river runoff from the three largest Russian rivers (i.e., the Yenisei, Lena, and Ob Rivers); however, that relationship was strongly dependent on the precipitation dataset used [5]. It has been suggested that this relationship is the result of changes in winter precipitation, which can accumulate as snowpacks in river basins and change the terrestrial water storage (TWS) during winter. It is thus important to evaluate the changes in TWS in river basins. In cold regions, TWS changes can be a primary factor in the variability of river runoff [6–8].

Meanwhile, Huang et al. [9] used results from the Fifth Coupled Model Intercomparison Project (CMIP5) to show that aridity in eastern Siberia, Alaska, and northern Canada will increase during this century and enhance the global warming trend. Therefore, an evaluation of the spatiotemporal variability in TWS in the Arctic is needed to better understand and quantify the hydrological changes that could occur in the next few decades. Suzuki et al. [10] recently analyzed the spatiotemporal variability in the Arctic TWS further and showed that between August 2002 and August 2015, the coastal tundra in the upper Lena River basin dried due to increased evapotranspiration rates resulting from severe summer warming. In addition, Nitze et al. [11] analyzed high-resolution Landsat data from 1999 to 2014 and suggested that regional patterns in changes to the areas of lakes have been declining since 1999 in the Alaska North Slope, Western Alaska, and the Kolyma Lowland regions, although this was not true for central Yakutia. Their limited analysis covered only 1.4% of the Arctic regions broadly categorized as tundra, suggesting that there could recently have been a wider trend toward decreasing lake coverage across the Arctic tundra. To understand the hydrological changes taking place throughout the pan-Arctic tundra, it is necessary to extend TWS analysis towards the entire region.

Within pan-Arctic river basins, most subsurface TWS consists of continuous permafrost. As soil freezes in the autumn, it preserves the imprints of the climatic conditions throughout the winter [6–9]. Iijima et al. [12] showed that permafrost warming in eastern Siberia abruptly increased the active water depth, which could cause changes in subsurface flows and degrade permafrost in continuous permafrost regions. However, despite recent advances [13], the mechanism by which the distribution of permafrost affects TWS and river runoff in large pan-Arctic river basins remains unclear.

Global Land Data Assimilation System v1 (GLDAS1) products and newly produced reanalysis data from GLDAS v2 (GLDAS2) have been widely and effectively used to understand the temporal and spatial variabilities of TWS anomalies. Recently, Wang et al. [14] studied three Chinese river basins using estimates based on TWS data from the Gravity Recovery and Climate Experiment (GRACE) and GLDAS to compare products based on GLDAS1 and GLDAS2. They showed that bias corrections in the precipitation data based on the latter greatly reduced the biases relative to that based on the former. However, they also noted that the latter had larger mean absolute errors. Thus, it is important to assess the availabilities of products based on GLDAS1 and GLDAS2 for the Arctic tundra and pan-Arctic river basins in order to investigate better products with which to analyze TWS anomalies in the regions.

Here, we present a thorough examination of spatiotemporal variability and forcing in the TWS across the entire Arctic circumpolar tundra region, and in the catchments of the Lena, Yukon, and Mackenzie Rivers, from April 2002 to December 2016. The study is structured as follows. Firstly, we present an extended analysis of GRACE-based TWS anomalies to detect changes in the entire pan-Arctic tundra region and their relevant causes. Secondly, we create a multi-model ensemble of reanalyzed data from GLDAS1 and GLDAS2 products to characterize the pan-Arctic TWS component with respect to various forcings such as temperature, precipitation, evapotranspiration, river runoff and inundation extent area data. Thirdly, we provide an assessment of basin-scale variations in TWS among the Lena, Yukon, and Mackenzie River basins, three of the largest in the

pan-Arctic region, and examine the relationship between the TWS and freshwater river runoff into the Arctic Ocean after 2002.

The paper is organized as follows. Section 2 describes the Methodology, including the data and theory. Section 3 presents the results, Section 4 is dedicated to discussion, and Section 5 concludes the study.

2. Methodology

2.1 Study area

Figure 1(a) shows a map of the Arctic circumpolar tundra region (ACTR), which we defined using GLDAS and vegetation data obtained from the 1° GLDAS2/Noah Dominant Vegetation Type datasets (https://ldas.gsfc.nasa.gov/gldas/GLDASvegetation.php) using the NOAHv3.3 vegetation dataset from GLDAS2. In the GLDAS, tundra regions are divided into two distinct types: mixed tundra and wooded tundra. In this study, we only present data for wooded tundra in order to avoid uncertainties associated with identifying mixed tundra along the narrow coastal areas of the Arctic Ocean, where it is difficult to distinguish between the ocean and land due to the coarse spatial resolution of GRACE data. In addition, we exclud from our analysis the areas in the ACTR that are within 300 km of glaciers and ice sheets (the masked-out areas in Figure 1 (a)) in order to remove the effects of glacial and ice sheet melt on the TWS anomalies. As a consequence, in our analysis, the ACTR is delineated by the regions represented in green in Figure 1a. We therefore obtained a land area of approximately 5,527,630 km^2 for the ACTR.

We calculated the distribution of permafrost throughout the ACTR based on data obtained from the National Snow and Ice Data Center (NSIDC) website [15]. Approximately 83% of the ACTR is covered by continuous permafrost, while the rest is covered by discontinuous or sporadic permafrost (Figure 1(c)).

To understand the effects of river runoff on the TWS anomalies, we conduct an analysis of large pan-Arctic rivers at the basin scale. Long-term river runoff data are limited for large pan-Arctic river basins; however, data exist for three large catchments (Figure 1(b) and Table 1) that are suitable for an analysis of basin-scale, long-term trends in river runoff and of the TWS between 2002 and 2016. The first catchment is the Lena River Basin in eastern Siberia of the Russian Federation, which has an area of approximately 2,430×10^3 km^2 that is comprised largely of continuous permafrost (71%). The second is the Yukon River basin in Alaska, which has an area of 850×10^3 km^2; it is covered by both continuous permafrost (23.2%) and discontinuous permafrost (74.7%). The third catchment is the Mackenzie River basin in northern Canada, which covers an area of 1,790×10^3 km^2, 20.0% of which is covered by continuous permafrost and 39.2% is covered by discontinuous permafrost.

Table 1. Characteristics of the three largest pan-Arctic river basins.

River basin	Gauge station	Drainage area (km^2)	Continuous permafrost (%)	Discontinuous permafrost (%)	Tundra coverage (%)
Lena River	Kusur	2,430×10^3	81.6	17.6	5.0
Yukon River	Pilot	850×10^3	23.2	74.7	19.5
Mackenzie River	Arctic Red River	1,790×10^3	20.0	39.2	33.8

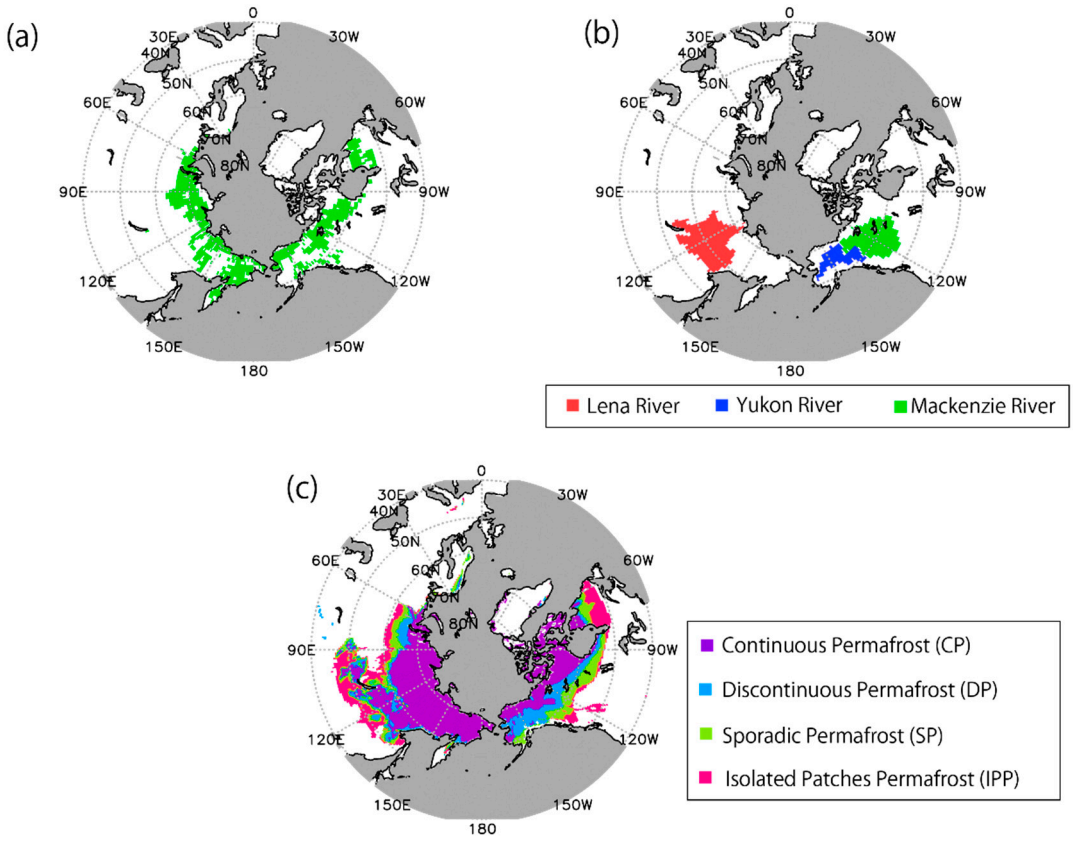

Figure 1. Maps of the study sites. (a) The Arctic circumpolar tundra region (ACTR), (b) the largest pan-Arctic river basins, and (c) the permafrost distribution.

2.2 Data

2.2.1 Satellite Data

To quantify the TWS in the study region, we obtained GRACE data (Level-2, Release 5) from three analysis centers: the University of Texas Center for Space Research (CSR) and the Jet Propulsion Laboratory (JPL) in the U.S.A. and the GeoForschungZentrum Potsdam (GFZ) in Germany. Each dataset consists of 158 monthly datasets collected between April 2002 and December 2016 spanning 15 Northern Hemisphere winters. Gaps in the dataset exist for 20 months during this time: June 2002, July 2002, June 2003, January 2011, June 2011, May 2012, March 2013, August 2013, September 2013, February 2014, July 2014, December 2014, June 2015, October 2015, November 2015, April 2016, September 2016, and October 2016. These gaps are due to instrumental problems and battery management issues (see the GRACE Science Data System Monthly Report June 2017). Here, we did not apply any interpolation to cover the periods of data loss. In our analysis, we use the ensemble mean of the three GRACE datasets (i.e., a simple arithmetic mean of the CSR, JPL and GFZ datasets) as recommended by Sakumura et al. [16] and the official GRACE Science Data System. In doing so, we are able to reduce random errors and enhance common signatures included within each GRACE dataset.

The GRACE data used in this study express the Earth's gravity field in the form of spherical harmonic coefficients (Stokes coefficients). These Stokes coefficients are estimated up to a degree and order of 60 or 96 depending on the analysis center and observation period. Here, we truncated the Stokes coefficients at a degree and order of 60 (corresponding to a spatial resolution of ~300 km), since the higher-frequency coefficients are especially contaminated by short wavelength noise from temporal aliasing errors [17]. In addition, we used filtering techniques to further reduce sources of short wavelength noise. We applied a Gaussian filter with a radius of 240 km.

Since GRACE measurements are less sensitive to the global-scale components of the Earth's gravity field, in particular, the degree-1 and zonal degree-2 components, which represent geocenter motion and the Earth's dynamic oblateness, respectively, it is a common practice to complement these components with other space geodetic techniques or model estimates. Here, we used the degree-1 coefficients estimated by combining GRACE data with an ocean model [18] and the zonal degree-2 coefficients measured via satellite laser ranging (SLR) [19]. Subsequently, we converted the GRACE data into surface mass variations using the methods presented by [20]. A degree-1 load Love number (k_1) of 0.021 was then used to convert the GRACE reference frame (center of mass) into the center of the figure frame to make the data consistent with the GLDAS data [18]. Atmospheric and oceanic mass variations were removed during the processing of the original GRACE data. We also corrected the data for the effects of glacial isostatic adjustments, which contribute less than 2% to the GRACE signal within our region of interest [21], using the model proposed by [22]. The long-term averages of the Stokes coefficients were removed from the monthly solutions to provide the surface mass variations, which represent the TWS anomalies relative to the static field. Hereafter, we refer to these TWS anomalies as TWS, which includes surface and subsurface water masses. According to our error analysis, the data are accurate to +/- 1 mm year^{-1}.

2.2.2 Reanalysis Data

The GLDAS1 and GLDAS2 products [23] are used to calculate TWS anomalies and assess TWS estimates from GRACE data. In this study, to examine the uncertainty in the GLDAS1 products, we use a multi-model ensemble of GLDAS1 data consisting of four different land surface models: 1) the Noah land surface model (LSM) [24], 2) the Community Land Model (CLM) [25], 3) the variable infiltration capacity (VIC) model [26], and 4) the MOSAIC LSM [27]. Each product has a monthly time step and a spatial resolution of 1.0° × 1.0°. The TWS derived from the multi-model GLDAS1 ensemble is defined as TWS_{GLDAS1}. Its ensemble spread (standard deviation) provides a measure of the uncertainty in the land surface models of the GLDAS1 products. GLDAS2, which currently uses only the Noah LSM and employs the Princeton meteorological forcing dataset [28] as the only source of forcing data, was corrected using observation-based datasets of precipitation, air temperature, and radiation. Here, we applied a low-pass filter to the GLDAS1 and GLDAS2 data to truncate the spherical harmonic components at a degree and order of 60. Additionally, a Gaussian filter with a radius of 240 km was applied to the GLDAS1 and GLDAS2 data to adjust them to the same spatial resolution as the GRACE data.

2.2.3 River flow rate data (R)

Observed flow rate data for the estuaries of the three major pan-Arctic rivers (the Lena, Mackenzie, and Yukon Rivers) are used to analyze the basin-scale variations in the TWS. For the Lena River, we use observations provided by R-ArcticNet (developed and maintained by the University of New Hampshire) from 2002 to 2009 and by the AHYST.Lena dataset [29,30] from 2010 to 2011, while the Canadian hydrometric database (HYDAT) and the United States Geological Survey (USGS) website were used for the Mackenzie from 2002 to 2015 and Yukon Rivers from 2002 to 2016, respectively.

For the Lena River, the runoff data were obtained from the Kusur hydrological station, which is located near the mouth of the river at 70.70°N, 127.65°E. The runoff data for the Yukon and Mackenzie Rivers were obtained from gauge stations at the river mouths, namely, from the Pilot station (61.93°N, 162.88°W) in the Yukon River and the Arctic Red River station (67.46°N, 133.75°W) in the Mackenzie River.

2.2.4 Inundation Extent Area (IEA)

Variations of surface inundation extent areas (IEAs) among the regions are analyzed using data from the Global Inundation Extent from Multi-Satellites (GIEMS) database developed by [31,32] as a 25-km-resolution inundated area map with a monthly temporal resolution. This dataset has been

widely used and evaluated over the northern Arctic regions as in Papa et al. [33] and Frappart et al. [34]. To assess how variations in the surface water (mostly within inundation areas) among the regions were related to spatial changes in the TWS, we jointly compared the spatial changes in the TWS identified using variations in the GRACE data with the mean IEA for both July and August of each year (referred to as JA IEA). This represents the largest inundation area in these regions throughout the year.

2.3 Theory

In this section, we outline the theoretical basis of our analysis. To evaluate the monthly TWS from GRACE data, we use the water balance equation expressed for instance by Suzuki et al. [10], as follows:

$$\Delta TWS = \int P\,dt - \int E\,dt - \int R\,dt = \Delta \mathrm{SWE} + \Delta \mathrm{CS} + \Delta \mathrm{SM} + \Delta \mathrm{GW} + \Delta \mathrm{SW} \quad (1)$$

where P is the monthly precipitation (mm month^{-1}), E is the monthly evapotranspiration (mm month^{-1}), R is the monthly river runoff from the basin (mm month^{-1}), ΔSWE is the change in the snow water equivalent (mm month^{-1}), ΔCS is the change in the total amount of water within the canopy (mm month^{-1}), ΔSM is the change in the vertical accumulated soil moisture within the total soil layer (mm month^{-1}) ΔGW is the change in the groundwater or ice within the permafrost (mm month^{-1}), and ΔSW is the change in different surface water bodies (e.g., lakes, rivers and wetlands; mm month^{-1}). Hereafter, we refer to the TWS values determined using GRACE data as TWS$_{\mathrm{GRACE}}$.

The GLDAS-based TWS determination includes only ΔSWE, ΔCW, and ΔSM from equation (1). Because ΔCW is a minor factor, the TWS determined from the GLDAS data depends primarily on ΔSWE and ΔSM. Hereafter, we refer to the TWS values determined from the GLDAS1 and GLDAS2 products as TWS$_{\mathrm{GLDAS1}}$ and TWS$_{\mathrm{GLDAS2}}$, respectively, and the P and E values determined from GLDAS1 and GLDAS2 are accordingly referred to as P_{GLDAS1}, P_{GLDAS2}, E_{GLDAS1}, and E_{GLDAS2}.

2.4 Analysis

2.4.1. TWS changes across the arctic circumpolar tundra region

We analyze the temporal variations of TWS (i.e., from GRACE, GLDAS1, and GLDAS2) from 2002 to 2016 along with other variables (i.e., the temperature, precipitation, evapotranspiration, and IEA) for the entire ACTR. First, we examined the consistency among the TWS estimates from the GRACE, GLDAS1, and GLDAS2 datasets based on the coefficients of determination (R^2) and differences in the linear trends. Second, we analyzed the possible mechanisms for the changes in the mean annual TWS of the ACTR by comparing the TWS estimates against other hydrological and climate components. Note that the mean annual TWS is simply the average of available monthly TWS data over all possible years, because some monthly TWS data were missing from the overall dataset as shown in section 2.2.1. However, the mean annual TWS was not available for 2002, as insufficient data were available (less than nine months). We also analyze the spatial variations in the linear TWS trends to identify consistencies among the linear trends of TWS$_{\mathrm{GRACE}}$ and of various hydro-meteorological factors, such as the precipitation and evapotranspiration, from the GLDAS1- and GLDAS2-based products.

2.4.2. TWS changes among the three river basins

Similar to what is done over ACTR, we analyze the temporal variations of all variables from 2002 to 2016 among the three river basins similar to section 2.4.1. In this part, we also use river runoff data to explore the relationship between the TWS and river runoff. Based on previous work [10,35,36], we hypothesize that the conditions during the autumn and winter will affect river runoff in the subsequent year. To test this, we calculated the correlations between the TWS values from July

Preprints (www.preprints.org) | NOT PEER-REVIEWED | Posted: 8 December 2017 doi:10.20944/preprints201712.0049.v1

Peer-reviewed version available at Remote Sens. 2018, 10, 402; doi:10.3390/rs10030402

of one year and those from June of the following year along with those for the annual river runoff using available data. We calculated the monthly lag correlation coefficient (r_{LAG}) for the annual river runoff data between 2002 and 2011 for the Lena River; we also calculated r_{LAG} between 2002 and 2015 for the Mackenzie River using monthly TWS averages from September to December and annual river runoff estimates from the subsequent year as well as monthly TWS estimates from January to May and annual river runoff values for the same year.

3. Results

3.1 TWS in the Arctic circumpolar tundra

In this section, we present the updated TWS data series for the ACTR from 2002 to 2016 and assess the regional TWS variability.

3.1.1 Temporal variations in the TWS in the ACTR

Figure 2(a) illustrates the temporal variations in the monthly TWS estimates averaged across the ACTR from GRACE, GLDAS1, and GLDAS2 data. From 2002 to 2016, the GRACE, GLDAS1, and GLDAS2 TWS datasets exhibit negative trends of -1.8 mm year^{-1}, -1.6 mm year^{-1}, and -5.1 mm year^{-1}, respectively. TWS_{GRACE} and TWS_{GLDAS2} show the best agreement in the linear trends (r = 0.92, p < 0.0001), despite the larger seasonal amplitude in TWS_{GLDAS2} due to a larger winter TWS. These rates of decline exceed the uncertainty of -1.0 mm year^{-1} associated with TWS_{GRACE} and thus confirm the ability of the GRACE-based TWS data to reflect temporal trends in the ACTR.

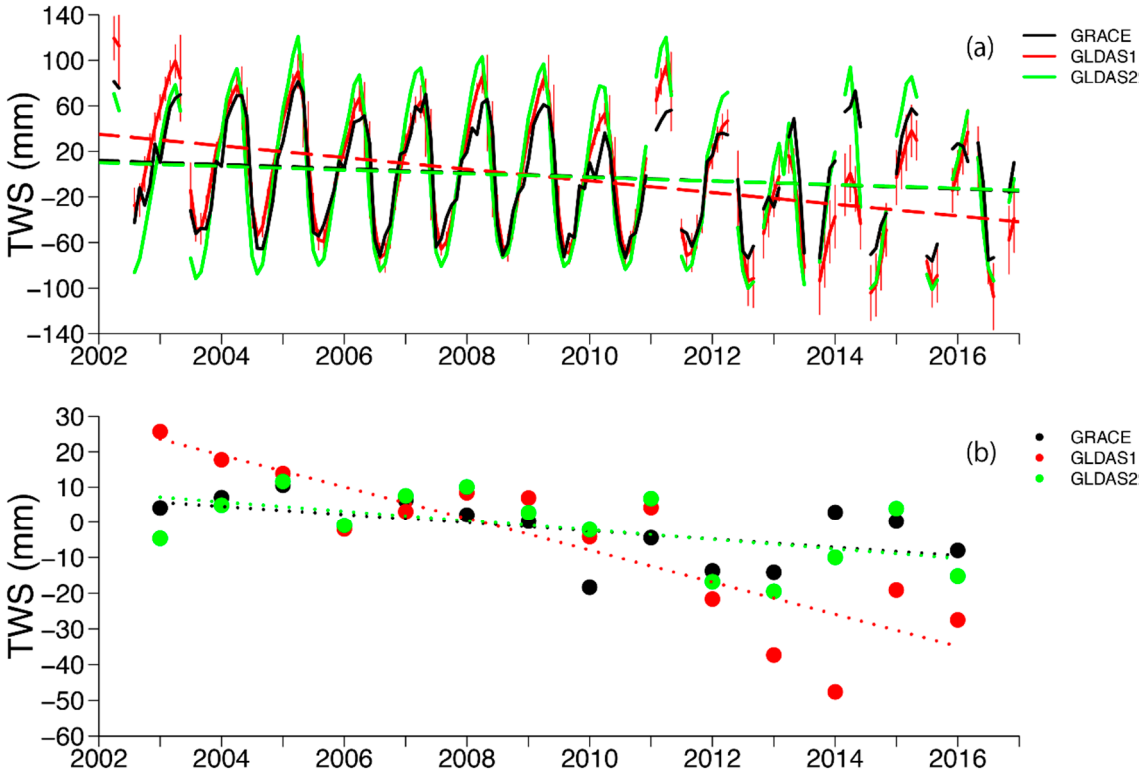

Figure 2. (a) Monthly and (b) annual temporal variations in the TWS anomalies in the Arctic circumpolar tundra region from 2002 to 2016. Long dashed and dotted lines denote the linear regression lines for the monthly and annual values, respectively.

The TWS_{GRACE} data are also highly correlated with TWS_{GLDAS1} (r = 0.90, p < 0.0001) despite the substantially larger rate of decline associated with GLDAS1 (-5.1 mm yr^{-1}). The values of R^2 between TWS_{GRACE} and TWS_{GLDAS1} (R^2 = 0.81, p < 0.0001) and between TWS_{GRACE} and TWS_{GLDAS2} (R^2 = 0.85, p < 0.0001) indicates the degree to which the variations can be explained with a linear model. Based on

these strong correlations among the three TWS datasets, we calculated a TWS change of more than 80% at the ACTR-scale using the GLDAS products, thus allowing us to determine the primary factor controlling the changes in TWS_{GRACE}. The similarities among the three datasets imply that, like TWS_{GLDAS1} and TWS_{GLDAS2}, TWS_{GRACE} also largely depends on the SWE and SM parameters. Even so, the negative trend in TWS_{GLDAS1} is nearly three times larger than the trends in TWS_{GRACE} and TWS_{GLDAS2}, which were very similar to each other. Overall, the inter-annual variation in TWS_{GRACE} can be best explained by the GLDAS2 dataset.

The mean annual TWS is plotted in Figure 2(b) for all years except 2002, when insufficient data were available (less than nine months). In these smoothed datasets, TWS_{GRACE} was again more strongly correlated with TWS_{GLDAS2} (r = 0.67, p = 0.009) than with TWS_{GLDAS1} (r = 0.50, p = 0.069). TWS_{GRACE}, TWS_{GLDAS1}, and TWS_{GLDAS2} decreased by -1.2 mm year^{-1}, -4.5 mm year^{-1}, and -1.3 mm year^{-1}, respectively. Thus, the long-term trends observed in the mean annual TWS_{GRACE} were most consistent with those observed in TWS_{GLDAS2}. Overall, these TSW data show a decline throughout the ACTR between 2002 and 2016, thereby providing evidence that hydrological changes are not only limited in the upper reaches of the Lena River basin as reported in [10] but also expanding throughout the whole ACTR.

3.1.2 Precipitation, Evapotranspiration, and air temperature from GLDAS and IEA.

Next, we present the monthly air temperature (T_a), precipitation (P), evapotranspiration (E), and IEA derived from the GLDAS1 and GLDAS2 datasets and assess their effects on the mean annual TWS_{GRACE} (Figure 3). The 2-m air temperatures in the ACTR from the GLDAS1 data are very close to those calculated from the GLDAS2 data (Figure 3(a), r = 1.0, p < 0.0001). However, GLDAS2 produced consistently higher P values than GLDAS1 (GLDAS1 – GLDAS2 = -11.4 mm, r = 0.77, p < 0.0001), while the inter-annual variability in E produced from GLDAS1 was larger than that observed from GLDAS2 (Figure 3(c), r = 0.96, p < 0.0001) due to higher (lower) values for E in summer (winter). However, these differences cancel out when we calculate the all-term averaged bias and are within the range of uncertainty associated with the various LSMs, as indicated by vertical red bars in Figure 3(c).

Preprints (www.preprints.org) | NOT PEER-REVIEWED | Posted: 8 December 2017 doi:10.20944/preprints201712.0049.v1

Peer-reviewed version available at Remote Sens. 2018, 10, 402; doi:10.3390/rs10030402

Figure 3. Temporal variations in the monthly hydro-meteorological factors, namely, the (a) 2-m air temperature(T_{aM}), (b) P, (c) E, and (d) IEA, of the Arctic circumpolar tundra region from 2002 to 2016.

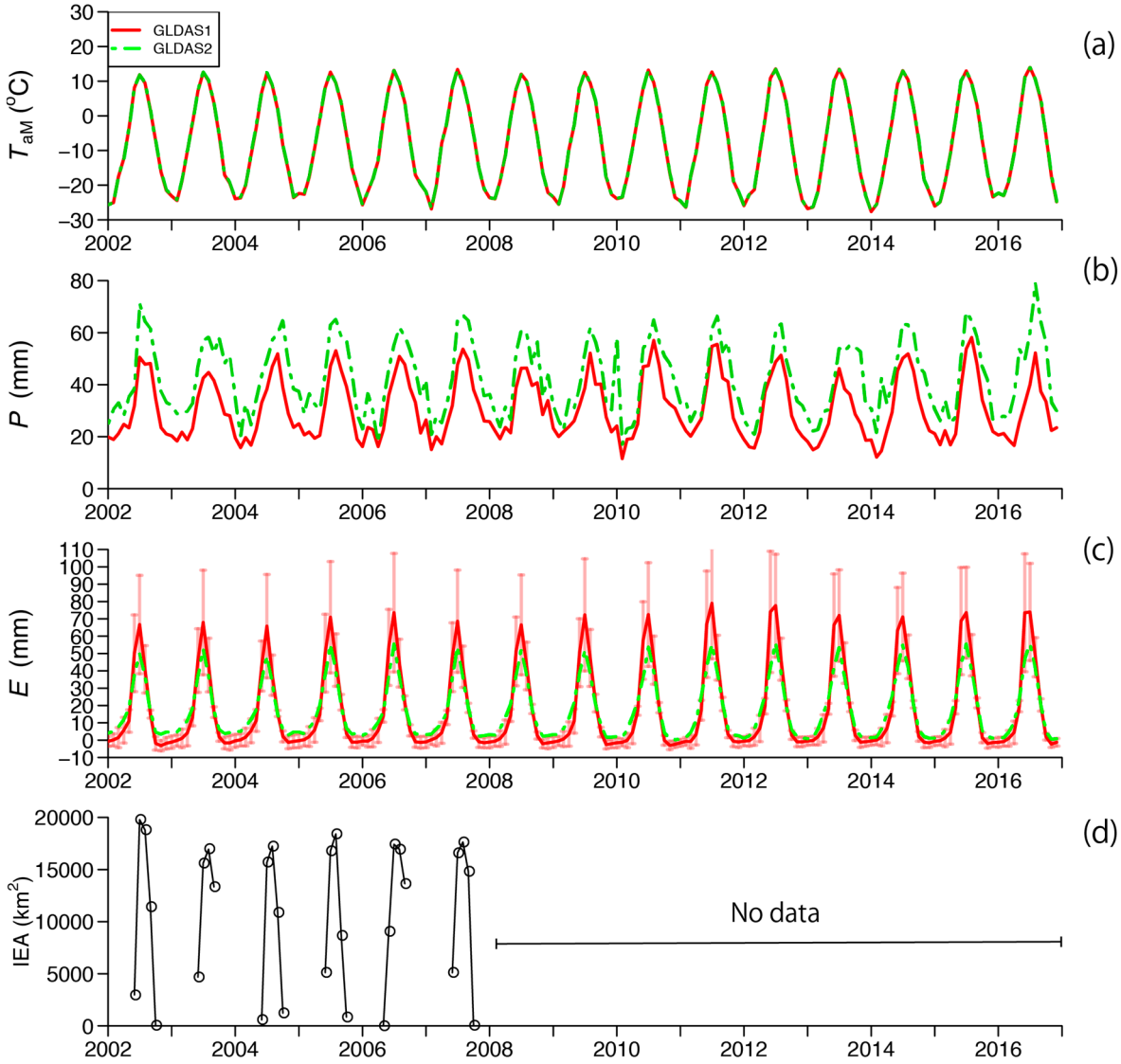

The temporal variations in the IEA (Fig. 3(d)) is characterized by large seasonal variations, with first inundations appearing in June and peaking in July or August before reducing to zero in October, when the surface water was either frozen or covered in snow.

3.1.3. TWS_{GRACE} vs. T_a, P, E and IEA

To identify the possible forcing mechanisms of the mean annual TWS in the ACTR, we compared the mean annual TWS_{GRACE} (Figure 2(b)) with the mean annual and summer (JJA) 2-m air temperature (Figure 4(a) and (b), respectively), the mean annual P (Figure 4(c)), the values of E (Figure 4(d)), and the summer IEA (Figure 4(e)). While there was no discernable trend in the mean annual temperature throughout the ACTR during this period, the JJA mean air temperature increased by approximately 0.12 °C $year^{-1}$, and one-third of the summer warming occurred in the upper part of the Lena River Basin [10]. However, no discernible trend was observed in P despite a slight decrease between 2005 and 2013.

Preprints (www.preprints.org) | NOT PEER-REVIEWED | Posted: 8 December 2017 doi:10.20944/preprints201712.0049.v1

Peer-reviewed version available at Remote Sens. 2018, 10, 402; doi:10.3390/rs10030402

Figure 4. Temporal variations in the annual hydro-meteorological factors, namely, (a) the mean annual (T_{aY}) and (b) mean JJA 2-m air temperature (T_{aJJA}), (c) P, (d) E, and (e) the JA IEA, of the Arctic circumpolar tundra region from 2002 to 2016. Dotted lines denote the linear regression lines for each colored element.

The GLDAS1- and GLDAS2-based E both increased steadily from 2002 to 2016 with slopes of approximately 4 mm year^{-1} for E_{GLDAS1} (r = 0.85, p < 0.001) and 1.2 mm year^{-1} for E_{GLDAS2} (r = 0.66, p = 0.008). The increase in E from either GLDAS dataset can explain most of the decrease in TWS_{GRACE} shown in Figure 4(a). The R^2 values between TWS_{GRACE} and the GLDAS1-based and GLDAS2-based estimates of E were approximately 0.72 and 0.43, respectively, indicating that E can explain 43% or 72% of the variation in TWS_{GRACE}.

The mean JA IEA shows a decrease between 2002 and 2006; overall, however, the mean JA IEA could not explain the decrease in TWS_{GRACE}. Thus, evapotranspiration driven by increasing summer temperatures denoted the primary factor controlling TWS_{GRACE}. This suggests that future warming might further decrease the TWS at high latitudes in the Arctic circumpolar region.

3.1.4 Regional trends in TWS, *P*, and *E*

Here, we consider the regional trends in the mean annual TWS, and P and E from both GLDAS1 and GLDAS2.

Figure 5(a) shows the spatial distribution of the trend in the annual TWS from 2002 to 2016 across the ACTR. There is an evident regional variation throughout the ACTR and a declining TWS in the high Arctic near the Lena River Basin. The trends shown in Figure 5(a) are statistically

Preprints (www.preprints.org) | NOT PEER-REVIEWED | Posted: 8 December 2017 doi:10.20944/preprints201712.0049.v1

Peer-reviewed version available at Remote Sens. 2018, 10, 402; doi:10.3390/rs10030402

significant ($p < 0.05$). Higher regression correlation coefficients are seen in the North American continent. In terms of regional changes in the TWS, a significant large negative trend in the TWS can be mainly seen in the region along the Gulf of Alaska and the Northwestern Territory in Canada. Meanwhile, the negative trends in the TWS in the Eurasian continent were weaker than those in the North American continent.

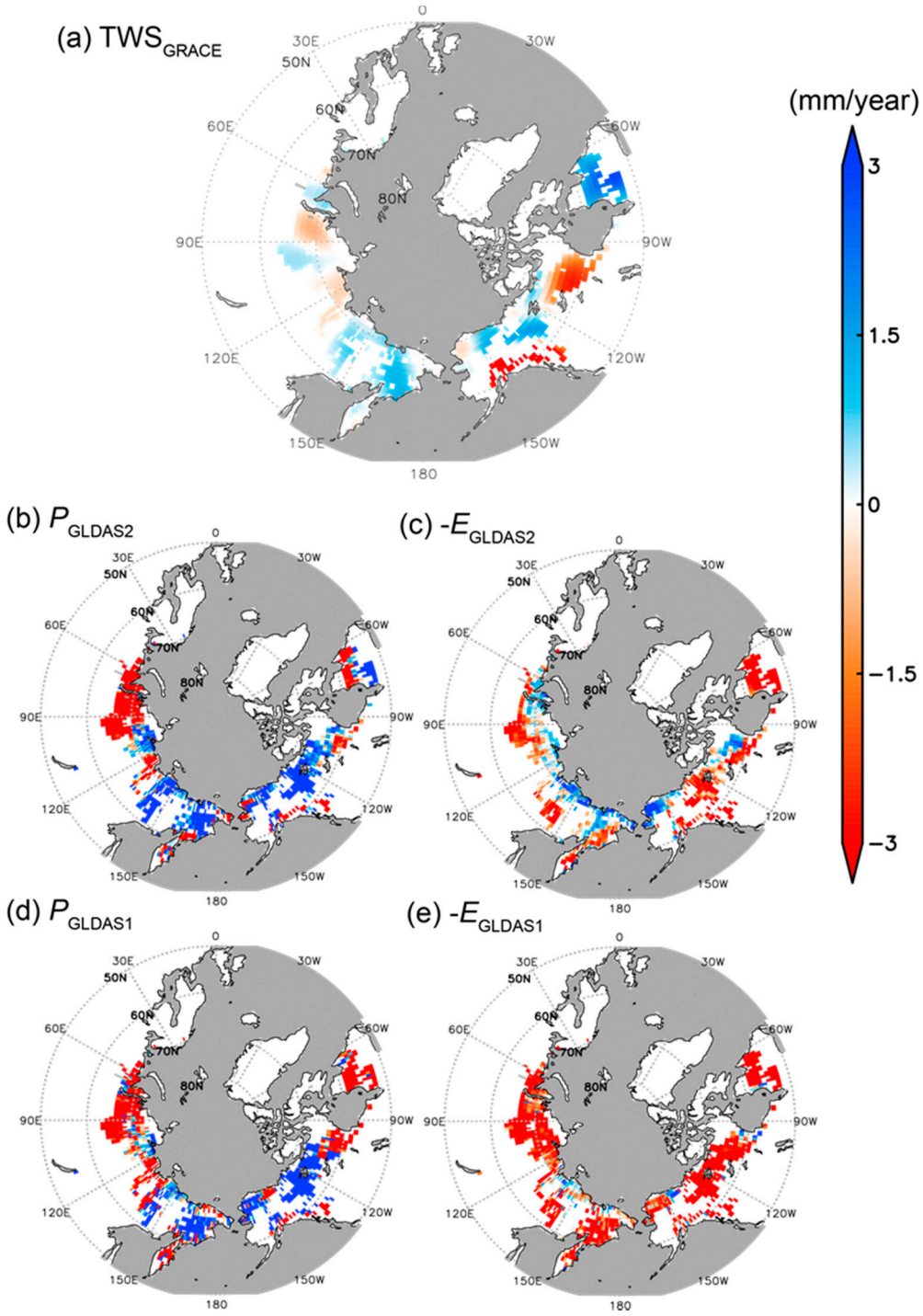

Figure 5. Spatial distribution of the slopes of temporal linear trends in each water balance component from 2002 to 2016 when $p<0.05$ (linear trend in TWS_{GRACE}). (a) TWS_{GRACE}, (b) P_{GLDAS2}. (c) $-E_{GLDAS2}$. (d) P_{GLDAS1}. (e) $-E_{GLDAS1}$.

To further understand these regional trends across the ACTR, we examined the distributions of P and E using the mean annual datasets from GLDAS1 and GLDAS2 (Figures 5(b) through (e)). The

spatial variations in P_{GLDAS1} and P_{GLDAS2}, and in E_{GLDAS1} and E_{GLDAS2} can be explained by the differences in the forcing data and in the land surface models in GLDAS1 and GLDAS2.

Table 2 lists the correlation coefficients between the linear trends of TWS_{GRACE} with the P and E estimates from both GLDAS1 and GLDAS2 according to the regions where TWS_{GRACE} either increased or decreased, as depicted in Figure 5(a). The results are further differentiated according to the magnitude of increase or decrease in TWS_{GRACE}, namely, values from 0 to 3 mm year^{-1} and values of greater than or equal to 3 mm year^{-1}. The strongest correlation coefficients are observed between TWS_{GRACE} and E for both GLDAS1 and GLDAS2, especially where TWS_{GRACE} had increased or decreased by more than 3 mm year^{-1}. This confirms that E dominates the spatial distribution of TWS_{GRACE}.

Table 2. Spatial correlation coefficients of the regional linear trends between TWS_{GRACE} and P or E.

Relationship of linear trends	Linear trend in TWS_{GRACE} is positive (≥ 3 mm year^{-1})	Linear trend in TWS_{GRACE} is positive (≥ 0 mm year^{-1})	Linear trend in TWS_{GRACE} is negative (< 0 mm year^{-1})	Linear trend in TWS_{GRACE} is negative (< -3 mm year^{-1})
TWS_{GRACE} & P_{GLDAS1}	-0.23	-0.16	0.07	0.03
TWS_{GRACE} & P_{GLDAS2}	0.13	0.20	0.16	0.18
TWS_{GRACE} & E_{GLDAS1}	0.33	0.31	-0.07	-0.10
TWS_{GRACE} & E_{GLDAS2}	0.59	0.55	-0.42	-0.44

Weaker correlations are observed between TWS_{GRACE} and P. This relationship is similar to the ACTR-averaged results in Figure 4. Similarly, P_{GLDAS2} and E_{GLDAS2} were more strongly correlated with TWS_{GRACE} than P_{GLDAS1} and E_{GLDAS1}.

Overall, these results suggest that changes in E throughout the ACTR were the primary driver of TWS_{GRACE} variations from 2002 to 2016. In addition, according to our analysis, we found that the GLDAS1-based TWS, P and E products exhibit poor correlations with the GRACE-based TWS. Thus, in the following sections, we use GLDAS2-based products only.

3.2 Confirmation of the IEA as a proxy for evapotranspiration

In the previous sections, we proposed that E was a principal driving factor in the spatiotemporal variations in TWS_{GRACE} by using GLDAS1 and GLDAS2 products. Here, we discuss additional evidence using IEA data as a proxy for evapotranspiration, since evapotranspiration has a direct effect on the extent of surface water (e.g., the IEA). To confirm the impacts of evapotranspiration on TWS_{GRACE}, we analyzed the similar spatiotemporal variabilities of TWS_{GRACE} and the JA IEA from 2002 to 2007. JA IEA data are available from 1997 to 2007, and thus, we compared these temporal variations for the period in which the TWS_{GRACE} data overlap with the JA IEA data. Figure 6 illustrates the long-term changes in TWS_{GRACE} and in the mean JA IEA between 2002 and 2007 and in the mean JA IEA from 1993 to 2007. Table 3 lists the correlation coefficients between TWS_{GRACE} and JA IEA according to the sign of change in the IAE. When the JA IEA increased between 2002 and 2007, TWS_{GRACE} (2002–2007) and the JA IEA (2002–2007) were strongly correlated (r=0.80). However, when the JA IEA decreased over time, the spatial correlation between TWS_{GRACE} and JA IEA from 2002 to 2007 was weaker (r=0.36). Thus, the temporal trends in the IEA are related to the temporal changes in TWS_{GRACE}. In addition, if we compare the regional trends in the JA IEA between 2002–2007 and 1993–2007, the spatial correlation coefficients between the 2002–2007 (0.83, when the IEA trends were positive) and 1993–2007 (0.56 when the IEA trends were negative) JA IEA data were very high regardless of whether the JA IEA trends were positive or negative.

Preprints (www.preprints.org) | NOT PEER-REVIEWED | Posted: 8 December 2017 doi:10.20944/preprints201712.0049.v1

Peer-reviewed version available at Remote Sens. 2018, 10, 402; doi:10.3390/rs10030402

387 **Table 3.** Spatial correlation coefficients of the linear trends between TWS$_{GRACE}$ and JA IEA.

Relationship of linear trends	Linear trend in the JA IEA (2002–2007) is positive	Linear trend in the JA IEA (2002–2007) is negative
TWS$_{GRACE}$ (2002–2007) & JA IEA (2002–2007)	0.80	0.36
JA IEA (2002–2007) & JA IEA (1993–2007)	0.83	0.56

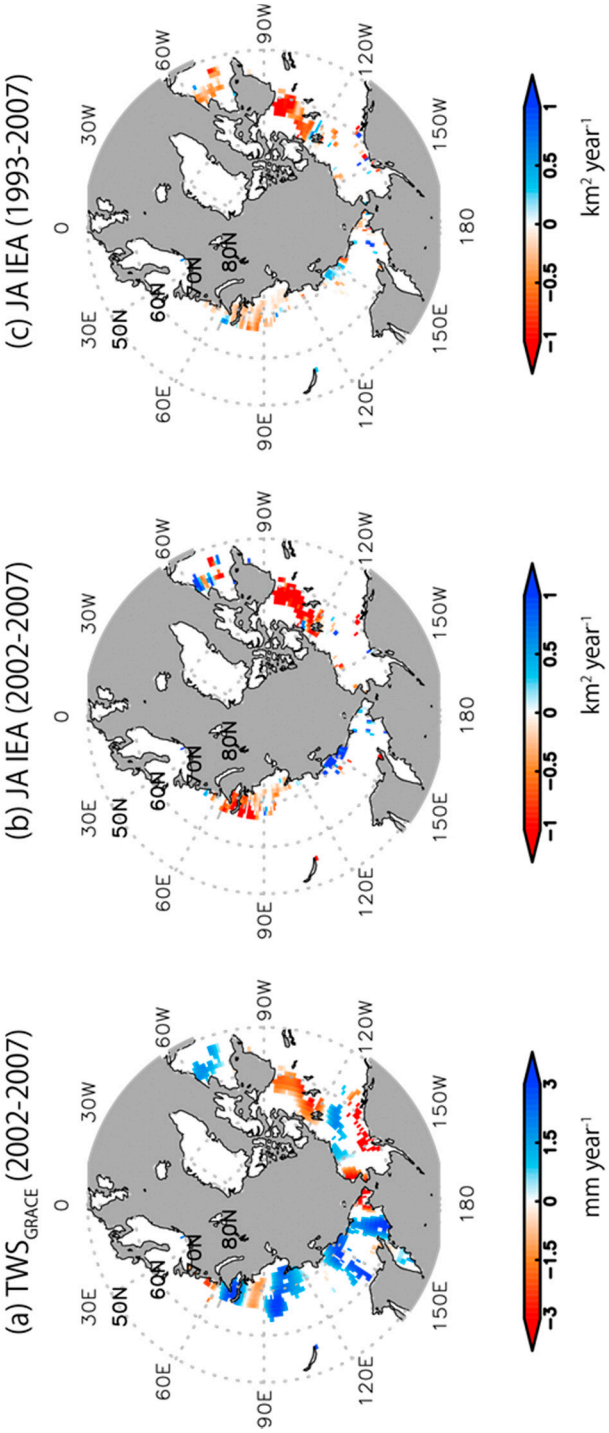

388

389 **Figure 6.** Spatial distribution of the slopes of temporal linear trends in the TWS anomalies and in the
390 IEA when p<0.05 (linear trend in TWS$_{GRACE}$). (a) TWS$_{GRACE}$ (2002–2007). (b) JA IEA (2002–2007). (c) JA
391 IEA (1993–2007).

Overall, the spatiotemporal variations in TWS_{GRACE} can be linked to changes in the IEA via changes in evapotranspiration. Thus, the results we obtained in this study can be supported by independent IEA data sets. Since evapotranspiration is probably responsible for the observed IEA variations (no precipitation changes are observed), and since the IEA contributes to the TWS variations and trends, our findings support the role of changes in *E* on the TWS trends.

3.3 Basin-scale variabilities in the TWS for three Arctic rivers

Here, we present the updated TWS data series for the Lena, Yukon, and MacKenzie Rivers and assess the variability in the TWS in relation to river runoff rates and other parameters.

3.3.1 Temporal variations

To evaluate the impacts of river runoff on three of the largest Arctic catchments, we analyzed basin-scale changes in TWS has changed since 2002 for the Lena, Yukon, and Mackenzie River basins (Figure 7). No significant trend is evident in either the Lena or Mackenzie Rivers, while a negative trend is observed in the Yukon River Basin.

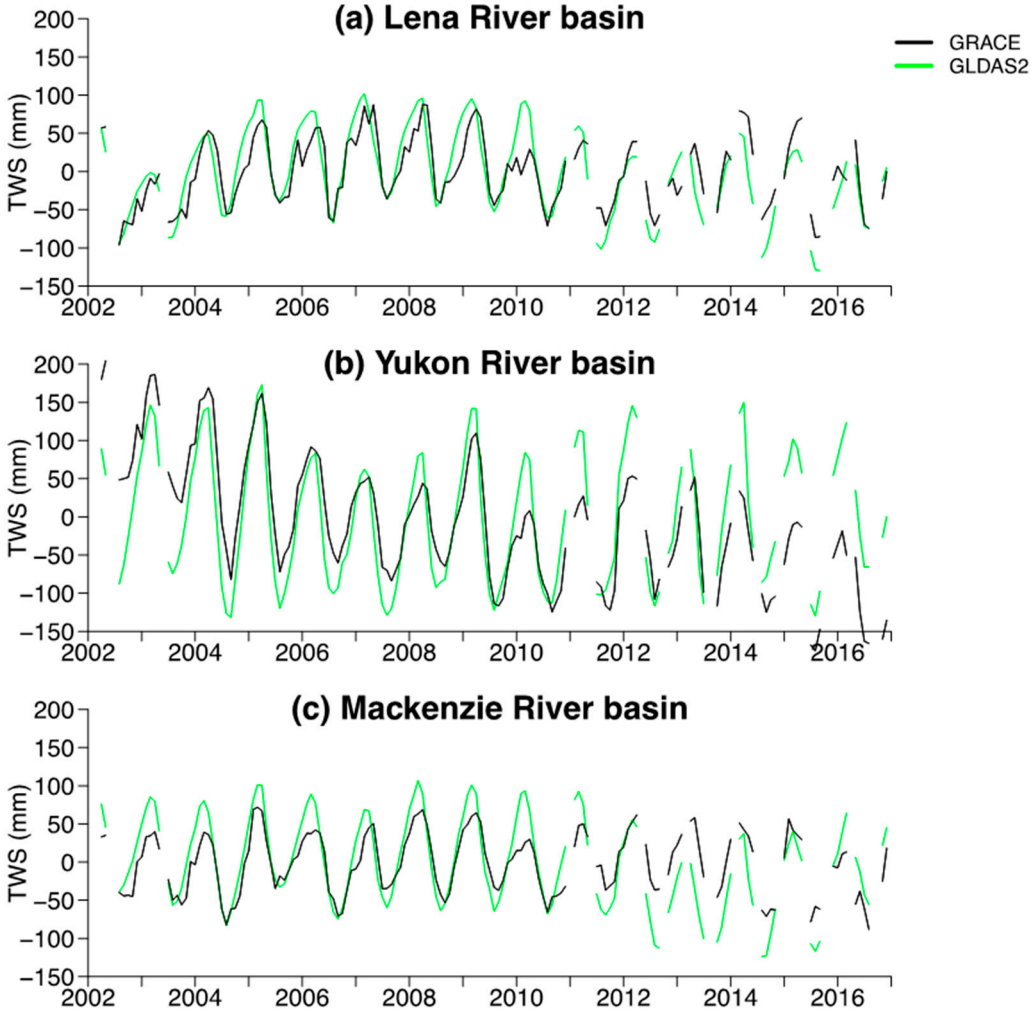

Figure 7. Temporal variations in the TWS among the largest pan-Arctic river basins from 2002 to 2016. (a) Lena River basin. (b) Yukon River basin. (c) Mackenzie River basin.

Preprints (www.preprints.org) | NOT PEER-REVIEWED | Posted: 8 December 2017 doi:10.20944/preprints201712.0049.v1

Peer-reviewed version available at Remote Sens. 2018, 10, 402; doi:10.3390/rs10030402

To understand the temporal variations in TWS_{GRACE}, we compared it to both TWS_{GLDAS1} and TWS_{GLDAS2}. As was observed for the entire ACTR, the correlation coefficients between TWS_{GRACE} and TWS_{GLDAS2} were the highest in the Lena River (r = 0.83), Yukon River (r = 0.72), and Mackenzie River (r = 0.80) basins.

3.3.2 Monthly mean *P* and *R*

Figure 7 shows the temporal variations in the monthly basin-averaged precipitation (P_{GLDAS1} and P_{GLDAS2}) and river runoff rates of each river basin. The maximum monthly *P* occurred in July for the Lena and Mackenzie River basins (Figure 8(a) and 8(c)) and in June or July for the Yukon River Basin (Figure 8(b)). The Lena River exhibits the largest amount of river runoff (*R*), followed by the Yukon River and then the Mackenzie River. The peak value of *R* occurred in June for all three rivers. The peak snowmelt occurs between April and June, accounting for approximately 40%, 36%, and 28% of the annual *R* in the Lena River, Yukon River, and Mackenzie River basins, respectively. The largest discrepancies in the precipitation between GLDAS1 and GLDAS2 are observed for the Yukon River. As shown in Figure 9, the monthly averaged *P* does not correspond to the monthly *R*.

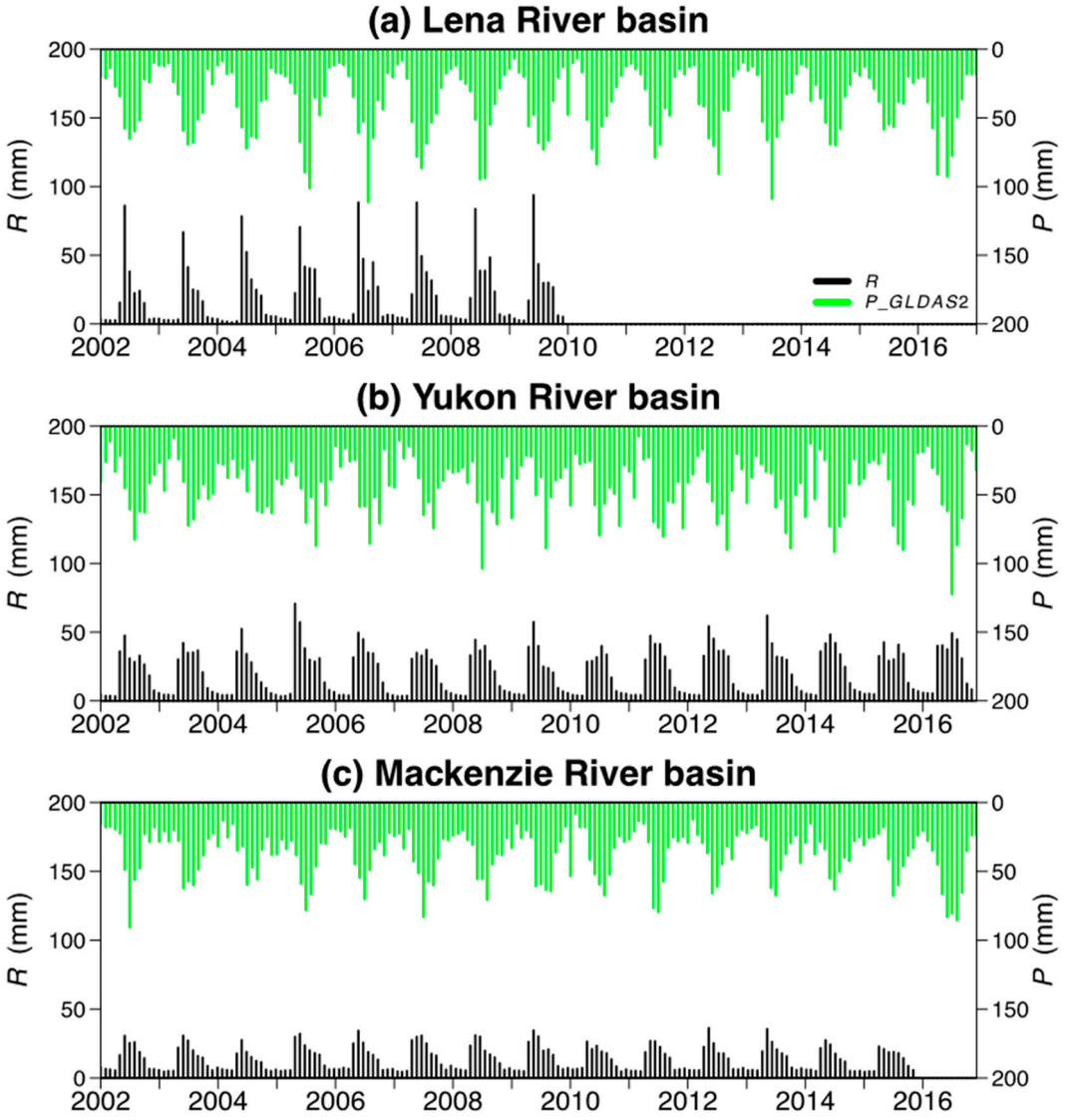

Figure 8. Temporal variations in the monthly water balance components from 2002 to 2016 in the (a) Lena River basin, (b) Yukon River basin, and (c) Mackenzie River basin.

Preprints (www.preprints.org) | NOT PEER-REVIEWED | Posted: 8 December 2017 doi:10.20944/preprints201712.0049.v1

Peer-reviewed version available at Remote Sens. 2018, 10, 402; doi:10.3390/rs10030402

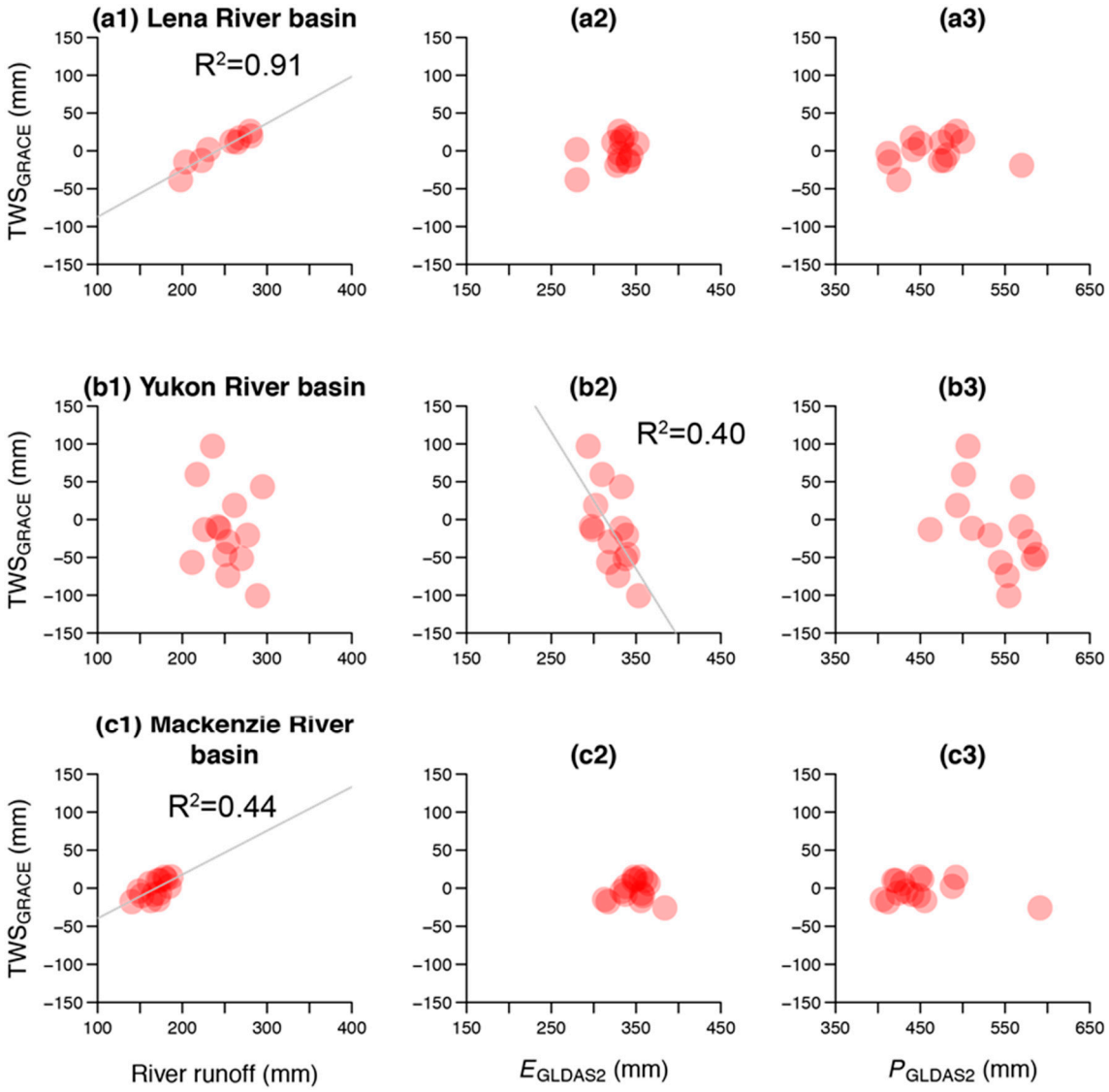

Figure 9. Relationships among the annual basin-scale TWS and the water balance components in the (a) Lena River basin, (b) Yukon River basin, and (c) Mackenzie River basin. Also shown are the (1) river runoff, (2) E_{GLDAS2}, and (3) P_{GLDAS2}. The gray lines denote linear regression lines when $p < 0.05$.

Comparing R with the TWS among the three river basins reveals strong positive correlations for the Lena River and Mackenzie River basins but no significant correlation for the Yukon River, where the TWS was sensitive to changes in E_{GLDAS2} (Figure 8). This confirms E as a driving factor for the decline in the TWS in the Yukon River catchment. Here, we consider only GLDAS2-based E data due to the greater consistency between the GLDAS2 and GRACE products.

3.3.3 Relationship between the TWS and runoff in the Lena and Mackenzie River basins

Here, we examine r_{LAG} as defined in section 2.4 to further investigate the correlation between the TWS and runoff in the Lena and Mackenzie River basins. We do not consider the TWS of the Yukon River basin, as it did not exhibit a correlation with the river runoff.

Statistically significant increases in r_{LAG} are observed in September in the Lena River Basin and April in the Mackenzie River Basin (Figure 10). The maximum r_{LAG} corresponds to the TWS in February for the Lena River Basin and in April for the Mackenzie River, suggesting that the conditions during the previous autumn and winter affected only the river runoff in continuous permafrost basins, such as those in the Lena River. In comparison, only a small portion of the Mackenzie River basin is covered by continuous permafrost, as nearly half of the basin is free of

permafrost. Therefore, the high r_{LAG} in the autumn within the Lena River Basin indicates that the autumn TWS can serve as a climatic signature for permafrost-dominated river runoff in any given year, as was noted previously by Suzuki et al. [10]. The influence on the autumn TWS from the preceding year is discernible, despite the inclusion of the snow water equivalent over the land. However, in basins such as the Mackenzie River, which are not dominated by permafrost, the TWS from the preceding year had no effect on the river runoff of the following year.

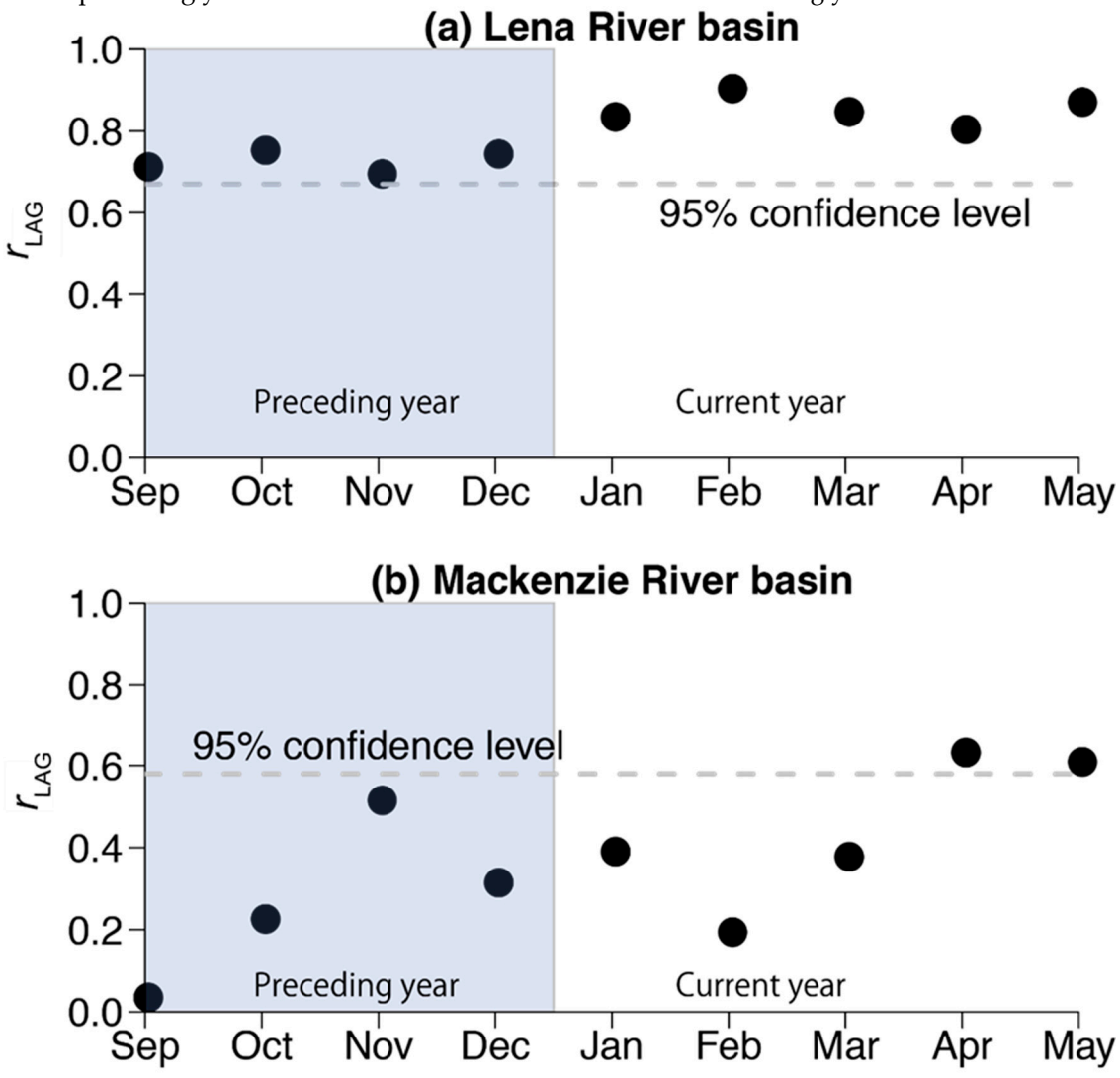

Figure 10. Seasonal variations in the monthly correlation coefficients r_{LAG} for different time-lagged values of the TWS. Dashed gray lines indicate the 95% confidence level. Shaded areas denote the preceding year in comparison with the river runoff of the current year.

4. Discussion

4.1 Hydrological changes in the tundra throughout the ACTR

Through our results, the GRACE-based TWS record shows a clear decrease in the TWS throughout the ACTR and that the JJA air temperature increased. The spatiotemporal variations in the TWS throughout the ACTR were related to the IEA, especially when the IEA increased. The weaker correlation between *E* and the IEA (i.e., when the IEA decreased) can be explained by subsurface processes, because all of the strong negative trends in the IEA can be observed in non-continuous permafrost zones that degraded rapidly. The previous GRACE-based TWS trends in eastern Siberia [21] and in the three largest Siberian river basins (i.e., the Lena, Yenisey, and Ob River basins) [37] all showed positive trends using shorter data periods (e.g., 5 or 8 years) than the present study. In addition, Huang et al. [9] showed that the aridity of most of the Artic region, including

eastern Siberia and the North American continent, will increase in this century using data from the CMIP5. Our results correspond to those of Huang et al. [9]. Furthermore, using the CMIP5 dataset, Cook et al. [38] demonstrated that the expansion of dry areas can be attributed to globally widespread increases in the potential evapotranspiration while the spatial heterogeneous response of the precipitation can be used to define the drying and wetting patterns over the global land surface. Their conclusions confirm our results, i.e., that the TWS in the ACTR is driven by increasing evapotranspiration. Thus, we propose that the TWS in the ACTR is driven by the IEA, which is correspondingly driven by increasing summer air temperatures and evapotranspiration. Some previous studies [39,40] showed that drying land can enhance land surface warming because of increased land surface temperatures under dry conditions. An increase in the aridity throughout the ACTR might accelerate the warming air temperature trend in the Arctic. Overall, our results have implications for understanding future trends in the TWS, which could be expected to continue to decline as the Arctic continues to warm due to climate change.

4.2 Basin-scale hydrological changes

Except for the Yukon River, we found a clear relationship between the TWS anomalies and river runoff. Walvoord and Kurylyk [13] showed that continuous permafrost prevents infiltration into the deeper soil layer while some of the subsurface water in discontinuous permafrost regions is connected to the groundwater and will thus increase the subsurface flow. Thus, all of the TWS accumulated during autumn and winter increases the amount of R in the Lena River Basin; however, continuous permafrost is scarce in the Mackenzie River basin, and most of the TWS can cause subsurface flow and change the TWS during a winter. Overall, as the continuous permafrost distribution decreases, the response of river runoff to precipitation will be accelerated and the role of the TWS as a climate record will be diminished.

Next, we discuss the possible causes for the GRACE-based TWS trend in the Yukon River basin. The Yukon River basin is located in a transition zone from continuous to discontinuous permafrost and is mostly covered by an unstable discontinuous permafrost zone. Nitze et al. [11] showed a net lake area loss of 2.8%, while Roach et al. [41] measured a lake area loss of 0.81% per year in western Alaska. In more continental areas, Necsoiu et al. [42] found an overall decreasing trend in the lake areas of 22 lakes and ponds from 1978 to 2005. The abundance of disappearing lakes in the discontinuous permafrost regions of Central Alaska [43] has been linked to an increased connectivity to the groundwater supply [44]. Permafrost degradation or disappearance along the continuous-discontinuous permafrost interface could represent a good explanation for the strong decreasing TWS trend in the Yukon River basin. The low correlation coefficient between TWS_{GRACE} and TWS_{GLDAS2} can be explained by permafrost degradation. Several research investigations [43,45,46] showed that an increased evapotranspiration was responsible for observed lake area losses in central Alaska, the Yukon Flats and the northwestern Canada. Those research results correspond well with our findings of a high correlation between the TWS and evapotranspiration and of no correlation between the TWS and river runoff in the Yukon River basin. Therefore, a negative trend in the GRACE-based TWS within the Yukon River basin and the low correlation coefficient between TWS_{GRACE} and TWS_{GLDAS2} can be explained by permafrost degradation and evapotranspiration, although further research is needed to investigate the details of the TWS changes in the Yukon River basin. Overall, permafrost degradation and increased evapotranspiration in the Yukon River basin could have caused the decreasing GRACE-based TWS trend from 2002 to 2016 because of the unstable discontinuous permafrost distribution throughout most of the Yukon River basin.

4.3 Inconsistencies between GLDAS1 and GLDAS2

Our analyses demonstrated a greater consistency between TWS_{GRACE} and the GLDAS2 product than the GLDAS1 data throughout the ACTR and in the largest pan-Arctic river basins.

However, there are also significant differences between the GLDAS products. For example, the values of P in GLDAS2 exceed those in GLDAS1, although the air temperatures are consistent

between the two products. Combined with the stronger spatial correlation coefficients between TWS_{GRACE} and P_{GLDAS2} (Table 2), we suggest that the GLDAS2 products are more suited for pan-Arctic hydrological analyses than GLDAS1. In addition, E_{GLDAS2} demonstrated a higher correlation with the spatial trends in the GRACE-based TWS. However, the linear trend in E_{GLDAS1} was much larger than that in E_{GLDAS2} with nearly ubiquitous negative trends over the ACTR. These results correspond with the results of Wang et al. [14], who showed that E_{GLDAS1} overestimated the evapotranspiration relative to E_{GLDAS2}.

However, one drawback with regard to the current GLDAS2 product is that it is based solely on the Noah LSM; meanwhile, GLDAS1 uses multiple land surface models. This allows GLDAS1 to provide greater evaluations of model uncertainties. For instance, E_{GLDAS2} falls within the ensemble spread of E_{GLDAS1} despite the different forcing data of GLDAS1 and GLDAS2. In addition, we found that the GLDAS1-based TWS using a sophisticated LSM (e.g., the CLM) had a much higher correlation with the GRACE-based TWS than that using a simple LSM utilizing a single-layer snow and vegetation model (e.g., the Noah LSM). Thus, the ensemble spread of the GLDAS1-based product reflects some parameter uncertainties in the LSMs. Moreover, the GLDAS1-based product using a sophisticated LSM could correspond more effectively to the GRACE-based TWS.

5. Conclusions

We present a record of the GRACE-derived TWS in the Arctic circumpolar tundra region (ACTR) and in the three largest pan-Arctic river basins from April 2002 to December 2016. Using the multi-model ensemble of reanalyzed data from GLDAS1 and the newly developed reanalyzed data from GLDAS2, including other key parameters such as T_a, P, E or remote-sensing based IEA, we find the following conclusions:

1. The negative trend in the TWS throughout the ACTR was primarily driven by evapotranspiration, which is accordingly driven by summer air temperatures as confirmed using the IEA. This negative trend could be expected to continue in the future due to further warming conditions during the summer season at high latitudes, leading to substantial reductions in the TWS throughout the Arctic. Meanwhile, precipitation has a very minor impact on the TWS.
2. In terms of regional changes in the TWS, a large and significant negative trend in the TWS can be observed mainly over the North American continent, including the region along the Gulf of Alaska and the Northwestern Territory of Canada. Meanwhile, the negative trends in the TWS over the Eurasian continent were weaker than those over the North American continent.
3. The TWS among the three river basins was further controlled by the presence of continuous permafrost. For example, the autumnal TWS in the Lena River Basin (which exhibits continuous permafrost) persisted through the winter of the following year. However, no such effect was observed in the Mackenzie River catchment, which is partially covered in both continuous permafrost and discontinuous permafrost.
4. The GLDAS2-based products corresponded better with the spatiotemporal variability in TWS_{GRACE} than the GLDAS1-based products. GLDAS2 is likely more suitable for analyzing hydrological changes in Arctic regions than GLDAS1.

Given the availability of river runoff data, our analysis of the relationship between river runoff and the TWS anomalies was limited to the three largest pan-Arctic river basins. To improve our understanding of the Arctic freshwater cycle, additional GRACE data regarding river runoff is required. In particular, the TWS_{GRACE} data in the Yukon River clearly indicated a negative trend in our analysis, and the data were not affected by river runoff. Although this corroborates the negative TWS trends as strongly related to evapotranspiration throughout the ACTR and in the Yukon River Basin, the mechanism for this is still unknown and should represent the focus of future research.

Supplementary Materials: No.

Acknowledgments: Portions of this study were supported by a Grant-in-Aid for Scientific Research (C) (No. 16K00581) and a Grant-in-Aid for Challenging Exploratory Research (no. 25550022). In addition, this study was

partly carried out by the Joint Research Program of the Institute for Space-Earth Environmental Research (ISEE), Nagoya University.

Author Contributions: K.S., K.I., Y.I. and T.H. conceived and designed this study; K.S. and K.M. analyzed the data; K.M., D. Y. and F.P. contributed materials and analysis tools; K.S., K.M., F.P., K.I., Y.I. and T.H. wrote the paper. All authors discussed and reviewed the manuscript.

Conflicts of Interest: The authors declare no conflict of interest. The founding sponsors had no role in the design of the study; in the collection, analyses, or interpretation of data; in the writing of the manuscript, and in the decision to publish the results.

References

1. Serreze, M.C.; Barrett, A.P.; Slater, A.G.; Woodgate, R.A.; Aagaard, K.; Lammers, R.B.; Steele, M.; Moritz, R.; Meredith, M.; Lee, C.M. The large-scale freshwater cycle of the Arctic. *J. Geophys. Res.* **2006**, *111*, C11010. doi:10.1029/2005JC003424.
2. Peterson, B.J.; Holmes, R.M.; McClelland, J.W.; Vörösmarty, C.J.; Lammers, R.B.; Shiklomanov, A.I.; Shiklomanov, I.A.; Rahmstorf, S. Increasing river discharge to the Arctic Ocean. *Science* **2002**, *298*, 2171–2173. doi:10.1126/science.1077445.
3. Shiklomanov, A.I.; Lammers, R.B. Record Russian river discharge in 2007 and the limits of analysis. *Environ. Res. Lett.* **2009**, *4*, 045015. doi:10.1088/1748-9326/4/4/045015.
4. Rawlins, M.A.; Ye, H.; YANG, D.; Shiklomanov, A.; McDonald, K.C. Divergence in seasonal hydrology across northern Eurasia: emerging trends and water cycle linkages. *J. Geophys. Res.* **2009**, *114*, D18119. doi:10.1029/2009JD011747.
5. Willmott, C.J.; Matsuura, K. Terrestrial air temperature and precipitation: monthly and annual time series (1950 - 1999). Available online: http://climate.geog.udel.edu/~climate/html_pages/README.ghcn_ts2.html (accessed on 17 Nov 2017).
6. Quinton, W.L.; Hayashi, M.; Pietroniro, A. Connectivity and storage functions of channel fens and flat bogs in northern basins. *Hydrol. Process.* **2003**, 17, 3665–3684. doi:10.1002/hyp.1369.
7. Papa, F.; Prigent, C.; Rossow, W.B. Monitoring flood and discharge variations in the Large Siberian rivers from a Multi-satellite technique. *Surv. Geophys.* **2008**, *29*, 297–317. doi:10.1007/s10712-008-9036-0.
8. Hood, J.L.; Hayashi, M. Characterization of snowmelt flux and groundwater storage in an alpine headwater basin. *J. Hydrol.* **2015**, *521*, 482–497. doi:10.1016/j.jhydrol.2014.12.041.
9. Huang, J.; Yu, H.; Guan, X.; Wang, G.; Guo, R. Accelerated dryland expansion under climate change. *Nat. Clim. Change* **2016**, *6*, 166–171. doi:10.1038/nclimate2837.
10. Suzuki, K.; Matsuo, K.; Hiyama, T. Satellite gravimetry-based analysis of terrestrial water storage and its relationship with run-off from the Lena River in eastern Siberia. *Int. J. Remote Sens.* **2016**, *37*, 2198–2210. doi:10.1080/01431161.2016.1165890.
11. Nitze, I.; Grosse, G.; Jones, B.; Arp, C.; Ulrich, M.; Fedorov, A.; Veremeeva, A. Landsat-based trend analysis of lake dynamics across northern permafrost regions. *Remote Sens.* **2017**, *9*, 640. doi:10.3390/rs9070640.
12. Iijima, Y.; Fedorov, A.N.; Park, H.; Suzuki, K.; Yabuki, H.; Maximov, T.C.; Ohata, T. Abrupt increases in soil temperatures following increased precipitation in a permafrost region, central Lena River basin, Russia. *Permafrost Periglac. Process.* **2010**, *21*, 30–41. doi:10.1002/ppp.662.
13. Walvoord, M.A.; Kurylyk, B.L. Hydrologic impacts of thawing permafrost—a review. *Vadose Zone J.* **2016**, *15*, 0. doi:10.2136/vzj2016.01.0010.
14. Wang, W.; Cui, W.; Wang, X.; Chen, X. Evaluation of GLDAS-1 and GLDAS-2 forcing data and Noah model simulations over china at the monthly scale. *J. Hydrometeor.* **2016**, *17*, 2815–2833. doi:10.1175/JHM-D-15-0191.1.
15. Ferrians, O.J., Jr; Heginbottom, J.A.; Melnikov, E.S. *Circum-Arctic Map of Permafrost and Ground-Ice Conditions (Version 2).* National Snow and Ice Data Center: Boulder, CO, USA, 2002.
16. Sakumura, C.; Bettadpur, S.; Bruinsma, S. Ensemble prediction and intercomparison analysis of GRACE time-variable gravity field models. *Geophys. Res. Lett.* **2014**, *41*, 1389–1397. doi:10.1002/2013GL058632.
17. Wahr, J.; Molenaar, M.; Bryan, F. Time variability of the Earth's gravity field: hydrological and oceanic effects and their possible detection using GRACE. *J. Geophys. Res.* **1998**, 103, 30205–30229. doi:10.1029/98JB02844.

18. Swenson, S.; Chambers, D.; Wahr, J. Estimating geocenter variations from a combination of GRACE and ocean model output. *J. Geophys. Res.* **2008**, *113*, 29077–29012. doi:10.1029/2007JB005338.
19. Cheng, M.; Tapley, B.D. Variations in the Earth's oblateness during the past 28 years. *J. Geophys. Res.* **2004**, *109*. doi:10.1029/2004JB003028.
20. Wahr, J.; Molenaar, M.; Bryan, F. Time variability of the Earth's gravity field: hydrological and oceanic effects and their possible detection using GRACE. *J. Geophys. Res.* **1998**, *103*, 30205–30229. doi:10.1029/98JB02844.
21. Velicogna, I.; Tong, J.; Zhang, T.; Kimball, J.S. Increasing subsurface water storage in discontinuous permafrost areas of the Lena River basin, Eurasia, detected from GRACE. *Geophys. Res. Lett.* **2012**, *39*. doi:10.1029/2012GL051623.
2. a, G.; Wahr, J.; Zhong, S.. Computations of the viscoelastic response of a 3-D compressible Earth to surface loading: an application to glacial isostatic adjustment in Antarctica and Canada. *Geophys. J. Int.* **2013**, *192*, 557–572. doi:10.1093/gji/ggs030.
23. Rodell, M.; Houser, P.R.; Jambor, U.; Gottschalck, J.; Mitchell, K.; Meng, C.-J.; Arsenault, K.; Cosgrove, B.; Radakovich, J.; Bosilovich, M.; *et al.* The Global Land data assimilation system. *Bull. Amer. Meteor. Soc.* **2004**, *85*, 381–394. doi:10.1175/BAMS-85-3-381.
24. Koren, V.; Schaake, J.; Mitchell, K.; Duan, Q.-Y.; Chen, F.; Baker, J.M. A parameterization of snowpack and frozen ground intended for NCEP weather and climate models. *J. Geophys. Res.* **1999**, *104*, 19569–19585. doi:10.1029/1999JD900232.
25. Dai, Y.; Zeng, X.; Dickinson, R.E.; Baker, I.; Bonan, G.B.; Bosilovich, M.G.; Denning, A.S.; Dirmeyer, P.A.; Houser, P.R.; Niu, G.; *et al.* The common land model. *Bull. Amer. Meteor. Soc.* **2003**, *84*, 1013–1023. doi:10.1175/BAMS-84-8-1013.
26. Liang, X.; Lettenmaier, D.P.; Wood, E.F.; Burges, S.J. A simple hydrologically based model of land surface water and energy fluxes for general circulation models. *J. Geophys. Res.* **1994**, *99*, 14415–14428. doi:10.1029/94JD00483.
27. Koster, R. D.; Suarez, M. J.; Laboratory for Atmospheres (Goddard Space Flight Center); Goddard Space Flight Center. Data Assimilation Office; U.S, L. F. H. P.; Goddard Space Flight Center. Climate and Radiation Branch Energy and water balance calculations in the Mosaic LSM. **1996**.
28. Sheffield, J.; Goteti, G.; Wood, E.F. Development of a 50-year high-resolution global dataset of meteorological forcings for land surface modeling. *J. Climate* **2006**, *19*, 3088–3111. doi:10.1175/JCLI3790.1.
29. Olga, M.; Nikita, T.; Lyudmila, L. Arctic Hydrology and Statistics for the Lena River basin. Compilative dataset on mean annual and extreme flows in the Lena River basin (compiled by Makarieva O., Tananaev N., Lebedeva L.), figshare, version 1.1 (04 August 2016), doi: 10.6084/m9.figshare.3206962
30. Tananaev, N.I.; Makarieva, O.M.; Lebedeva, L.S. Trends in annual and extreme flows in the Lena River basin, northern Eurasia. *Geophys. Res. Lett.* **2016**, *43*, 10764–10772. doi:10.1002/2016GL070796.
31. Prigent, C.; Papa, F.; Aires, F.; Rossow, W.B.; Matthews, E. Global inundation dynamics inferred from multiple satellite observations, 1993–2000. *J. Geophys. Res.* **2007**, *112*, 1147–1113. doi:10.1029/2006JD007847.
32. Papa, F.; Prigent, C.; Aires, F.; Jimenez, C.; Rossow, W.B.; Matthews, E. Interannual variability of surface water extent at the global scale, 1993–2004. *J. Geophys. Res.* **2010**, *115*, D12111. doi:10.1029/2009JD012674.
33. Papa, F.; Prigent, C.; Rossow, W.B. Ob' River flood inundations from satellite observations: a relationship with winter snow parameters and river runoff. *J. Geophys. Res.* **2007**, *112*, D18103. doi:10.1029/2007JD008451.
34. Frappart, F.; Papa, F.; Güntner, A.; Werth, S.; Ramillien, G.; Prigent, C.; Rossow, W.B.; Bonnet, M.-P. Interannual variations of the terrestrial water storage in the Lower Ob' Basin from a multisatellite approach. *Hydrol. Earth Syst. Sci.* **2010**, *14*, 2443–2453. doi:10.5194/hess-14-2443-2010.
35. Suzuki, K.; Kubota, J.; Ohata, T.; Vuglinsky, V. Influence of snow ablation and frozen ground on spring runoff generation in the Mogot Experimental Watershed, southern mountainous taiga of eastern Siberia. *Hydrol. Res.* **2006**, *37*, 21–29.
36. Suzuki, K. Estimation of snowmelt infiltration into frozen ground and snowmelt runoff in the Mogot experimental watershed in east Siberia. *IJG* 2013, 04, 1346–1354. doi:10.4236/ijg.2013.410131.
37. Muskett, R.R.; Romanovsky, V.E. Groundwater storage changes in arctic permafrost watersheds from GRACE and in situmeasurements. *Environ. Res. Lett.* **2009**, *4*, 045009. doi:10.1088/1748-9326/4/4/045009.
38. Cook, B.I.; Smerdon, J.E.; Seager, R.; Coats, S. Global warming and 21st century drying. *Clim. Dyn.* **2014**, *43*, 2607–2627. doi:10.1007/s00382-014-2075-y.

671 39. Whan, K.; Zscheischler, J.; Orth, R.; Shongwe, M.; Rahimi, M.; Asare, E.O.; Seneviratne, S.I. Impact of soil
672 moisture on extreme maximum temperatures in Europe. *Weather Clim. Extremes* **2015**, *9*, 57–67.
673 doi:10.1016/j.wace.2015.05.001.
674 40. Fu, Q.; Feng, S. Responses of terrestrial aridity to global warming. *J. Geophys. Res. Atmos.* **2014**, *119*, 7863–
675 7875. doi:10.1002/2014JD021608.
676 41. Roach, J.K.; Griffith, B.; Verbyla, D. Landscape influences on climate-related lake shrinkage at high
677 latitudes. *Glob. Change Biol.* **2013**, *19*, 2276–2284. doi:10.1111/gcb.12196.
678 42. Necsoiu, M.; Dinwiddie, C.L.; Walter, G.R.; Larsen, A.; Stothoff, S.A. Multi-temporal image analysis of
679 historical aerial photographs and recent satellite imagery reveals evolution of water body surface area and
680 polygonal terrain morphology in Kobuk Valley National Park, Alaska. *Environ. Res. Lett.* **2013**, *8*, 025007–
681 025017. doi:10.1088/1748-9326/8/2/025007.
682 43. Riordan, B.; Verbyla, D.; McGuire, A.D. Shrinking ponds in subarctic Alaska based on 1950-2002 remotely
683 sensed images. *J. Geophys. Res.* **2006**, *111*, 29–11. doi:10.1029/2005JG000150.
684 44. Yoshikawa, K.; Hinzman, L.D. Shrinking thermokarst ponds and groundwater dynamics in discontinuous
685 permafrost near council, Alaska. *Permafrost Periglac. Process.* **2003**, *14*, 151–160. doi:10.1002/ppp.451.
686 45. Lantz, T.C.; Turner, K.W. Changes in lake area in response to thermokarst processes and climate in Old
687 Crow Flats, Yukon. *J. Geophys. Res. Biogeosci.* **2015**, *120*, 513–524. doi:10.1002/2014JG002744.
688 46. Labrecque, S.; Lacelle, D.; Duguay, C. R.; Lauriol, B.; Hawkings, J. Contemporary (1951–2001) evolution of
689 lakes in the Old Crow Basin, Northern Yukon, Canada: remote sensing, numerical modeling, and stable
690 isotope analysis. *ARCTIC* **2009**, *62*.
691